

Self-Driving and Merging Droplets on Wettability Gradient Surfaces: A Lattice Boltzmann Study

Mehmet Alptuğ BOYLU¹, Umut CEYHAN^{*2}

¹ Graduate School of Natural and Applied Sciences, İzmir Kâtip Çelebi University, 35620, İzmir, Türkiye

² Department of Mechanical Engineering, İzmir Kâtip Çelebi University, 35620, İzmir, Türkiye

(Alınış / Received: 29.05.2023, Kabul / Accepted: 14.09.2023, Online Yayınlanma / Published Online: 25.12.2023)

Keywords

Interfacial flow,
Contact line,
Wettability gradient,
Lattice Boltzmann method

Abstract: Self-transport and control of droplets play an essential role in the development of microfluidic devices, self-cleaning, water harvesting, and heat transfer enhancement. Droplet manipulation without an external force can be accomplished if a wetting gradient is structured on surfaces. The contact angle hysteresis generates a driving force toward the more wetting side. If this force is balanced by the viscous stresses near moving contact lines, droplets on such surfaces may attain constant translational speed determined by this balance. The D2Q9 lattice Boltzmann method is employed for the simulation of the self-driven droplets on wettability gradient surfaces. By varying the surface energy and fluid viscosities, the behavior of single droplets on surfaces, their merging mechanism, and equilibrium shapes and motions within confined channels are studied systematically. If the droplet moves in a more viscous fluid, the droplet's speed dependence on the wetting gradient is observed to weaken. For large aspect ratio channel flows, it is shown that two-dimensional prediction of the interface motion approaches the three-dimensional D3Q19 model computations.

İslanabilirlik Gradyan Yüzeylerinde Kendi Kendini Yürüten ve Birleştiren Damlacıklar: Bir Lattice Boltzmann Çalışması

Anahtar Kelimeler

Arayüzey akışı,
Temas hattı,
İslanabilirlik gradyanı,
Lattice Boltzmann metodu

Öz: Damlacıkların kendi kendine taşınması ve kontrolü, mikroakışkan cihazların geliştirilmesinde, kendi kendini temizlemede, su toplamada ve ısı transferini geliştirmede önemli bir rol oynar. Yüzeylerde bir ıslatma gradyanı yapılandırılmışsa, harici bir kuvvet olmadan damlacık manipülasyonu elde edilebilir. Temas açısı histerezisi, daha çok ıslanan tarafa doğru bir itici güç oluşturur. Bu kuvvet, hareketli temas hatlarının yakınındaki viskoz gerilimlerle dengelenirse, bu tür yüzeyler üzerindeki damlacıklar, bu denge tarafından belirlenen sabit öteleme hızına ulaşabilir. Bu çalışmada D2Q9 lattice Boltzmann yöntemi, ıslanabilirlik gradyan yüzeylerinde kendiliğinden hareket eden damlacıkların simülasyonu için kullanılmıştır. Yüzey enerjisi ve akışkan viskoziteleri değiştirilerek, tek damlacıkların yüzeyler üzerindeki davranışı, bunların birleştirme mekanizması ve sınırlandırılmış kanallar içindeki denge şekilleri ve hareketleri sistematik olarak incelenmiştir. Damlacık daha viskoz bir akışkan içinde hareket ederse, damlacık hızının ıslanma gradyanına bağlılığının zayıfladığı gözlemlenmiştir. Büyük görünüm oranlı kanal akışları için, arayüz hareketinin iki boyutlu tahmininin üç boyutlu D3Q19 modeli hesaplamalarına yaklaştığı gösterilmiştir.

1. Introduction

Self-transport and manipulation of droplets are essential for many applications like microfluidic devices [1] and lab-on-a-chip systems [2], biomedical

applications [3], heat transfer enhancement [4], self-cleaning [5], to name a few [6]. For example, in heat transfer on surfaces, manipulation of droplets by wetting gradients is promising to increase the efficiency of heat transfer. The occurrence of

* Corresponding author: umut.ceyhan@ikcu.edu.tr

condensation either as film-wise condensation or drop-wise condensation affects the mechanism of heat transfer. Because the continuous film creates a resistance for heat transfer, dropwise condensation is more effective. But in high rates of temperature differences, it cannot be possible to observe dropwise condensation [4,7].

The manipulation of the interfaces, however, is possible by playing with the wettability of the surfaces. This change in the surface wetting may provide self-propulsion (passive control) which is a preferred mechanism since it does not require external forcing (active control). The idea of changing the wettability of surfaces can be utilized to vary the droplet speed [8], the orientation by combining it with a liquid infusion or lubricant impregnation [9,10], the size [11], to control water droplet motion by varying the wall energy [12] or topography [13], etc.

When a liquid droplet is placed on a surface that is atomically smooth and chemically homogeneous, the contact angle between the liquid-vapor interface and the surface is unique. The existence of imperfections due to surface roughness and/or energy distribution, however, alters this uniqueness. The droplet may attain an equilibrium shape, pin (depin) to (from) structures, and move due to hysteresis [14]. For example, if the surface is more wetting (more prone to spreading out) at one end than at the other, the droplet tries to move towards the more wetting end. This happens because the liquid spreads more and makes a larger contact area with the solid substrate at the more wetting end, which can cause the droplet to be pulled towards that direction due to capillary forces [15,16]. In other words, the droplet moves from the low-surface energy side towards the high-surface energy side because the liquid particles are attracted more onto the high-surface energy substrates (more wetting) than the low-surface energy substrates (less wetting). The motion is also possible if a wedge like wettability patterning exist on the surfaces [17,18].

A gradient on the surface wettability generates a driving force. It is known that self-transport is faster for low-surface tension fluids like ethanol compared to water as it is more wetting [19,20] on a fixed substrate. But without altering the surface tension of the droplet, its shape or motion can be controlled by varying the surface energy of the surfaces [21]. Geometric gradients like the self-motion of droplets on conical surfaces are also possible (see, e.g., Ding et al. 2023 [22]). Assisted by both surface gradients and wetting gradients, a droplet may further be accelerated. Recently, Raj et al. 2023 [23] utilize wetting gradient for controlled water collection, Xie et al. 2023 [24] discuss switchable wettability patterns for the spontaneous and controlled motion of droplets and subaqueous bubbles, and Sung et al. 2023 [25] fabricate 3D printed wetting gradient surfaces to minimize splashing of water droplets.

The lattice Boltzmann method is one of the numerical methods to be able to integrate the governing equations controlling the motion of two-phase systems. In this paper, the lattice Boltzmann method is used for simulating the model problems because of the method's mobility for wetting problems. This mesoscopic numerical method is capable of solving a wide range of problems from simple fluids to complex chemical reactions and has lower computing cost due to its step-by-step solution (i.e., no requirement of matrix inversion), compared to traditional methods such as Finite Volume Method, Finite Element Method, Boundary Element Method, etc.

The purpose of this study is to consider only the gradient in the surface energy for droplet manipulation by using the Lattice Boltzmann Method and to propose how to use wetting gradients to manipulate such interfaces either as single or multiple droplets. The following is believed to be novelty of this study: (i) the mechanisms of self-motion for droplets on surfaces and confined between two surfaces are explained, (ii) the droplet can be moved to or merged at a desired location, (iii) the effect of the viscosity ratio on the motion for both single and merging droplets is also discussed, (iv) the plane model which is considered in this study can be used as a guide for three-dimensional interfaces, especially for confined droplets within large aspect ratio channels.

In the following sections, first the numerical method is introduced and various problems are analyzed for validation purposes. Then, the mechanisms of self-driven single or multiple droplets on and within chemically structured surfaces are discussed.

2. Material and Method

2.1. Numerical Method

Lattice Boltzmann method is a mesoscopic numerical integration method for fluid dynamics which comes from the discretization of the Boltzmann equation. It defines the behavior of a gas or liquid at this level by expressing the evolution of particle distribution functions on a lattice grid. These distribution functions describe the chances that particles travelling at particular velocity will be present at each lattice location. The method controls the temporal evolution of these distribution functions as a result of particle advection and collisions. The D2Q9 model is a specific lattice Boltzmann method that uses a two-dimensional lattice with nine discrete velocity vectors, and it provides a wide range of fluid flow simulations.

D2Q9 model is capable of capturing the thermodynamic variations, such as temperature and pressure, by introducing a free energy functional into the Boltzmann equation. This functional represents the total energy of the system, including both kinetic

and potential energy, and can be used to compute quantities such as the equation of state, heat capacity, and surface tension along the drop interface γ_{LV} [26].

To implement the free energy in the D2Q9 model, firstly, distribution functions are defined, which describe the probability of finding a particle with a particular velocity at a given point in space and time. These distribution functions are then evolved using the Boltzmann equation, which takes into account the collision of particles and their interactions with the surrounding fluid.

Binary fluid is modeled by a Landau free energy functional. The free energy density, ϕ , is introduced into the Boltzmann equation by adding a term that represents the change in free energy due to the collision of particles. The bulk free energy density $\phi(\phi)$ as function of fluid density ρ , order parameter (phase) ϕ , is given as [27]

$$\phi(\phi) = \frac{c^2}{3}\rho\ln\rho + a\left(-\frac{1}{2}\phi^2 + \frac{1}{4}\phi^4\right). \quad (1)$$

In equation (1), c is the lattice velocity parameter defined as $c = \frac{\Delta x}{\Delta t}$, a is constant affecting the surface tension and interface width. Equation (1) enables binary phase separation as $\phi = \pm 1$. The governing equations modeling the motion of fluid particles as continuity and Navier-Stokes are recovered with LBM by using Chapman-Enskog expansion [28]. In the continuum regime, the continuity (equation (2)) and linear momentum balances (equation (3)), in index notation, are

$$\partial_t \rho + \partial_k (\rho v_k) = 0, \quad (2)$$

$$\partial_t (\rho v_j) + \partial_k (\rho v_k v_j) = -\partial_k P_{kj} + \partial_k [\eta (\partial_j v_k + \partial_k v_j)] + \rho F_j, \quad (3)$$

where ρ is the fluid density, v is the fluid velocity, η is the dynamic viscosity of fluid, P_{kj} is the pressure tensor and F_j is the body force. In equations (2) and (3), j is free while the k is dummy indices, respectively. For two-dimensional problems $j, k=1,2$ and for three-dimensional problems $j, k=1,2,3$. In modeling two-phase flows (binary systems), two distribution functions are utilized as $f_i(\mathbf{r}, t)$ and $g_i(\mathbf{r}, t)$. Distribution function f recovers the physical properties and g recovers order parameters. Because of the D2Q9 model that is used, there exist nine directions with subscript i defining the directions varying from 1 to 9. The directions are given as [26]

$$\mathbf{e} = [0,0; 1,0; -1,0; 0,1; 0,-1; 1,1; -1,-1; -1,1; 1,-1]. \quad (4a)$$

For the three-dimensional models, however, D3Q19 model is used with nineteen directions which in its vector form is defined as [29]

$$\mathbf{e} = [0,0,0; 1,0,0; -1,0,0; 0,1,0; 0,-1,0; 0,0,1; 0,0,-1; 1,1,0; -1,1,0; 1,-1,0; -1,-1,0; 0,1,1; 0,-1,1; 0,1,-1; 0,-1,-1; 1,0,1; -1,0,1; 1,0,-1; -1,0,-1]. \quad (4b)$$

In this case, the subscript i for the distribution functions varies from 1 to 19. The vectors in equations (4a) and (4b) are the lattice velocity vectors for $c=1$.

Physical parameters can be found by using distribution functions as in equation (5) below.

$$\rho = \sum_i f_i, \phi = \sum_i g_i, \rho v = \sum_i f_i e_i \quad (5)$$

The distribution functions are evolved in time by collision and streaming steps. In equations (6) and (7), collision and streaming steps are shown in one equation.

$$f_i(\mathbf{r} + e_i \Delta t, t + \Delta t) = f_i(\mathbf{r}, t) - \mathbf{M}^{-1}[\mathbf{S}(\mathbf{M}[f_i - f_i^{eq}])] \quad (6)$$

$$g(\mathbf{r} + e_i \Delta t, t + \Delta t) = g_i(\mathbf{r}, t) - \frac{1}{\tau_\phi} [g_i - g_i^{eq}] \quad (7)$$

where τ_ϕ is relaxation parameter. Multiple-Relaxation Time (MRT) operator is used for the collision equation in (6) where the collision term $[f_i - f_i^{eq}]$ is multiplied with $\mathbf{M}^{-1}\mathbf{S}\mathbf{M}$. It gives more accurate results due to having more than two parameters as free and tunable parameters and possible choice for the matrices \mathbf{M} and \mathbf{S} , distribution functions f_i^{eq} and g_i^{eq} and details of the LBM implementation can be found in the study of Pooley et al. [30] and of Boylu [31].

To satisfy the no-slip boundary conditions on the walls, the mid-way bounce back technique is utilized and wetting boundary condition is provided by setting the wall normal gradient of the order parameter ϕ [26].

2.2. Validation

The problems that are interested in this study are affected greatly by the contact line dynamics. The contact angle between the liquid-vapor interface and the surface determines the statics and dynamics of the problem. To this end, the solver is validated for both static and dynamic problems.

The problem setup is shown in Figure 1. For single droplets, the bottom surface interacts with the droplet on which the surface energy is varied. The top surface is away from the droplet. For the confinement effect, the top surface touches the droplet interface. The left and right ends of the domain are treated as periodic. The number of lattices in both directions varies for different problems. The green color represents the droplet as fluid 1 and the blue color represents the

outside fluid as fluid 2. The number of lattices in x and y directions vary for different problems.

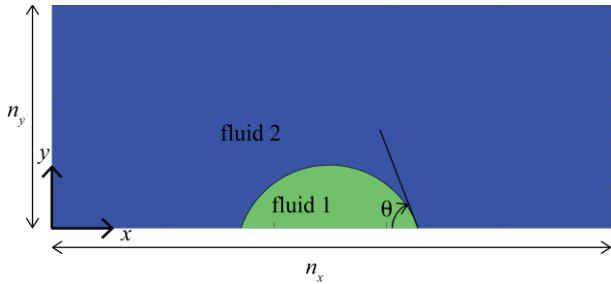


Figure 1. Problem domain, n_x and n_y are the number of lattices used along x and y directions, the contact angle θ may be unique or different at both contact lines

For droplets on surfaces with uniform surface energy, the computed angles and Laplace pressures are measured at the equilibrium state for several wettabilities. By setting the normal gradient of the phase field (order parameter) at the surface, it is possible to define the equilibrium contact angles. If there is deformation, the dynamic angles are determined as part of the solution which deviate from the equilibrium angle. The measured contact angles and shape of the droplets are shown in Figure 2.

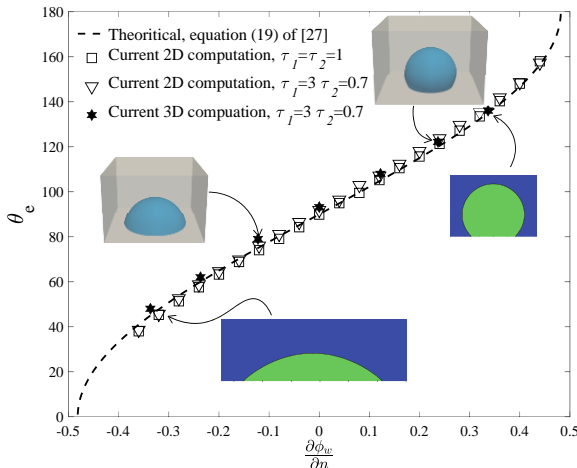


Figure 2. The variation of measured contact angles with respect to normal gradient of ϕ at the wall. The dashed line is theoretical relation [27], squares are for $\tau_1 = \tau_2 = 1$, lower triangles are for $\tau_1 = 3, \tau_2 = 0.7$. The insets show representative equilibrium profiles for partial wetting cases

The pressure difference across the interface at equilibrium is also measured and validated: Balancing forces normal to an interfacial element, the pressure difference in an out of a droplet is balanced by the resultant force per unit area due to uniform surface tension γ between droplet and exterior fluid. This uniform surface tension force in the normal direction is determined by $\gamma \nabla \cdot \mathbf{n}$ with \mathbf{n} being unit normal from droplet to outside fluid. The divergence of the unit normal for a spherical droplet of radius r is $2/r$. This shows that the pressure difference across such interface scales as $p_d - p_o \sim \gamma/r$ where p_d is the pressure inside the droplet, p_o is the outside pressure. The slope determines the surface tension.

Two different tau parameter pairs are used to validate different viscosity ratio fluids that is studied later. While τ_1 determines the kinematic viscosity of fluid 1, τ_2 determines the kinematic viscosity of fluid 2. The viscosity ratio, λ , is defined as the ratio of kinematic viscosity of fluid 1 to fluid 2. The use of MRT technique provides better predictions when the viscosity ratio of the two phases is different than unity. The theoretically computed relation between the wall-normal gradient of ϕ and the wetting angle agrees with the numerically computed angles. The dynamic motion of interfaces within capillary channels is also compared [30]. The details about contact angle tuning and dynamic validations can be found in Boylu [31].

3. Results

3.1. Motion of droplets on wettability gradient surfaces

Small droplets for which the gravitational forces are negligible are considered and, in this section, their motion driven by surface energy gradients is studied. To be able to explain the source of this driving mechanism, first, the equilibrium contact angles of droplets on surfaces which do not provide motion are defined. The simplest of such cases is substrates with uniform surface energy around the contact line in equilibrium. This does not require the surface energy to be uniform everywhere if there is pinning at a physical roughness. For clean surfaces, the contact angle is defined by the Young value. The contact angles at the left and right of the center of mass of a droplet are defined as

$$\cos(\theta_e^l) = \frac{\gamma_{SV}^l - \gamma_{SL}^l}{\gamma}, \quad \cos(\theta_e^r) = \frac{\gamma_{SV}^r - \gamma_{SL}^r}{\gamma}, \quad (8)$$

where γ_{SV} is the surface tension at the solid-vapor interface and γ_{SL} is the surface tension at the solid-liquid interface.

The results presented are all in lattice units in this and following subsections. The domain length is set to $n_x = 500$ and height to $n_y = 50$. The motion is initialized by placing the droplet of radius 30 lattice units at $x = 50$ as a semi-circle by using a linear wettability gradient reducing from θ_e^{left} to θ_e^{right} . When the surface energy of the surface at which the droplet contacts is non-uniform, the contact angles at the two triple junctions are different. If there were any equilibrium state, the angles would be equilibrium angles that can be called as θ_e^l and θ_e^r (as defined in equation (8)). The wetting gradient and inequality of the contact angles initiate the motion of the droplet. Due to hysteresis, it is known that the dynamic angle would be less than the equilibrium angle if the contact line recedes; it would be more if the contact line advances. For a negative wetting gradient surface, the left contact line tries to attain a larger contact angle

compared to the right contact line. When the left contact line recedes, because the contact angle is smaller than the equilibrium angle, the following inequality holds:

$$\gamma_{SV}^l - \gamma_{SL}^l > \gamma \cos(\theta_e^l). \quad (9)$$

When the right contact line advances, on the other hand, as the advancing contact angle is greater than the equilibrium one there, the corresponding inequality becomes

$$\gamma_{SV}^r - \gamma_{SL}^r > \gamma \cos(\theta_e^r). \quad (10)$$

Summation of the surface tension forces at the two contact lines, then, requires

$$\gamma_{SV}^r - \gamma_{SL}^r - (\gamma_{SV}^l - \gamma_{SL}^l) > \gamma [\cos(\theta_e^r) - \cos(\theta_e^l)] > 0 \quad (11)$$

for $\theta_e^{left} > \theta_e^{right}$, as is the case for negative wetting gradient surface. This generates a net force in positive x -direction which moves the droplet toward the right. One could also design a surface with a positive wetting gradient and this would drive the motion toward the left. In other words, the difference in the contact angles results in a Laplace pressure gradient along the interface, this pressure difference drives the motion.

It is also possible to obtain a scaling law for the droplet speed. When the droplet reaches a terminal speed, ϑ_d , the driving force due to wetting gradient and the viscous forces computed at the base of the droplet are in balance. The spreading coefficient S is defined as

$$S = \gamma_{SV} - \gamma_{SL} - \gamma. \quad (12)$$

When $S < 0$, the fluid termed as partial wetting and equation (12) can also be defined in terms of the Young value as

$$S = \gamma(\cos \theta_e - 1). \quad (13)$$

For slender droplets, the speed of the droplet on small wetting gradients, with the use of (13), scales as

$$\vartheta_d \sim \frac{h_c}{\eta} \frac{dS}{dx} = \frac{h_c \gamma}{\eta} \frac{d \cos \theta_e}{dx} \approx \frac{h_c \gamma}{\eta} \theta_e \frac{d\theta_e}{dx} \quad (14)$$

where h_c is the height and η is the dynamic viscosity of the droplet, respectively. The driving force explained above is balanced by the viscous stress mostly near the moving contact lines. In the small slope regime, the viscous stress can be computed with lubrication theory with no-shear stress condition at the droplet interface and this balance determines the moving speed [32]. For a droplet moving with constant speed ϑ_d , it scales linearly with $\frac{d\theta_e}{dx}$ for fixed h_0 corresponding to the equilibrium angle $\theta_e(x_c)$ measured at x_c (middle of droplet).

In Figure 3, the droplet speed variation with wetting gradient is shown (measured in degrees per unit lattice length) for different wettability gradients obtained by varying the wetting angle at the left of the domain (θ_e^{left}), as $150^\circ, 135^\circ, 120^\circ, 90^\circ, 60^\circ$, and keeping the one at the right of the domain (θ_e^{right}) fixed at 30° . The viscosity ratio used for validation shown in Figure 2 obtained by setting $\tau_1 = 3, \tau_2 = 0.7$. This sets λ approximately to 12.4. In Figure 3, we set $\tau_1 = 3$, and vary τ_2 to see the viscosity ratio effect.

The droplet moves with a constant speed and it varies linearly with the wetting gradient for $\lambda = 10$ and for the wetting angles studied: $30^\circ \leq \theta_e \leq 150^\circ$. It should be noted that the equilibrium angle approaches 30° toward the end of the domain for all the cases and the theoretical prediction is valid for small angles and large viscosity ratios.

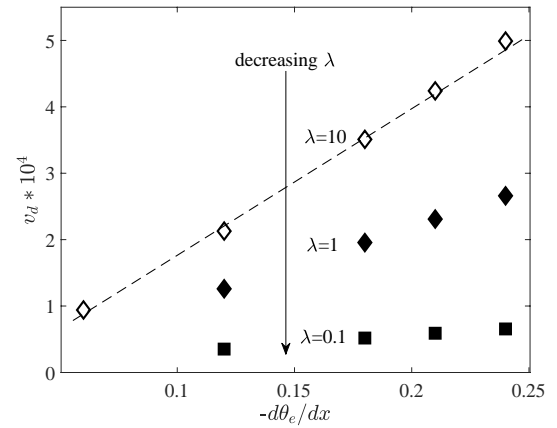


Figure 3. Variation of droplet speed as a function of wetting gradient. Hollow diamonds ($\lambda=10$) are the terminal speeds for various wetting gradients, dashed line is shown to emphasize the linearity; filled diamonds ($\lambda=1$) and filled squares ($\lambda=0.1$) shows the effect of the viscosity ratio

One would expect, however, the droplet to slow down if the viscosity of the outside fluid is increased. To show this effect, more cases with viscosity ratios of $\lambda=0.1, 1$ are studied. This variation is shown on the same plot with filled diamonds and filled squares with a clear observation of the slowing down of the droplet if it moves in a more viscous fluid. Furthermore, as λ decreases, the dependence of the droplet speed on the wetting gradient weakens.

3.2 Merging of droplets

Motivated by the simple idea of the previous subsection, it is possible to move droplets toward each other and merge. A proposition is made here as a possible use in self-cleaning, water harvesting or heat transfer enhancement applications. For example, one could merge small droplets which are able to resist gravity on car shields or windows, merge by the wetting gradient. This would increase the effective bond number (ratio of gravitational forces to surface tension forces) [33] of the merged droplet and for

sufficiently large volumes, it would move downwards with the aid of gravity. In another example, the merged droplets could be transported directionally depending on the gradients of the wetting patterns on the substrate. It is also shown that for the merging, the size of the droplet can be different. To this end, two droplets on the substrate are placed as shown in Figure 4. The gradients are set to be symmetric with respect to $x = x_0$ (mid of the domain) with a gradient of $2(\theta_e^{left} - \theta_e^{right})/n_x$. The number of lattices in x and y directions, n_x and n_y , are set to 250 and 100, respectively, with droplet radii of 30 in lattice units. The history of droplet motion is shown in panels (a) to (d) of Figure 4 for equal size droplets. In panels (e) to (h) of the same figure, the merging of different size droplets is shown. As can be seen from the velocity vectors (only the asymmetric case is shown as it is more intriguing), the outside fluid is squeezed by the motion of the two droplets and leaves the gap at an oblique path due to asymmetry. After the merge, the free surface attains its equilibrium shape; again, at a later time shown in panel (i), the deformation of the interface toward a circular arc is observed; the velocity is maximum at the location where the interface is away from the equilibrium.

To check the influence of the viscosity ratio, λ is varied from 0.83/0.067 to 0.1 and 1. It is observed that the droplets slow down due to the increased shear stress on the interface. The droplets move in a more viscous fluid, but eventually, they merge and attain the same equilibrium shape.

The change in the gradient of the wetting would change the speed and the time for the coalescence, as shown in the previous section; however, it would not affect the idea of merging droplets at a desired location to increase the effective bond number.

This proposition of such wetting gradients used in the merging of droplets drives further motivation to stop the motion of a droplet at a desired location. It is, finally, postulated that the self-motion of a droplet stops at x_0 , with the aid of symmetrically structured gradient walls with respect to the stopping location, x_0 . For motion from left to right, while the upstream wetting gradient is $d\theta_e/dx$ from $x=0$ to x_0 , it should be $-d\theta_e/dx$ downstream.

3.3. Confinement effect

When the droplet considered here is confined from the top with a wall as well as the bottom, it wets both surfaces. For uniform surface energy surfaces, the droplets attain an equilibrium shape which can be called as a fluid column. Because the contact angles of the interfaces are the same at all triple junctions, the shape of the interface becomes a circular arc meeting the walls at the wetting angle. The shape of any contact angle is determined by the geometry. Because the curvature of radius of the interfaces are the same, the

pressure jumps across the interfaces are the same and there is no pressure difference to drive the droplet in the confinement. However, generating a wettability gradient surface can trigger the motion.

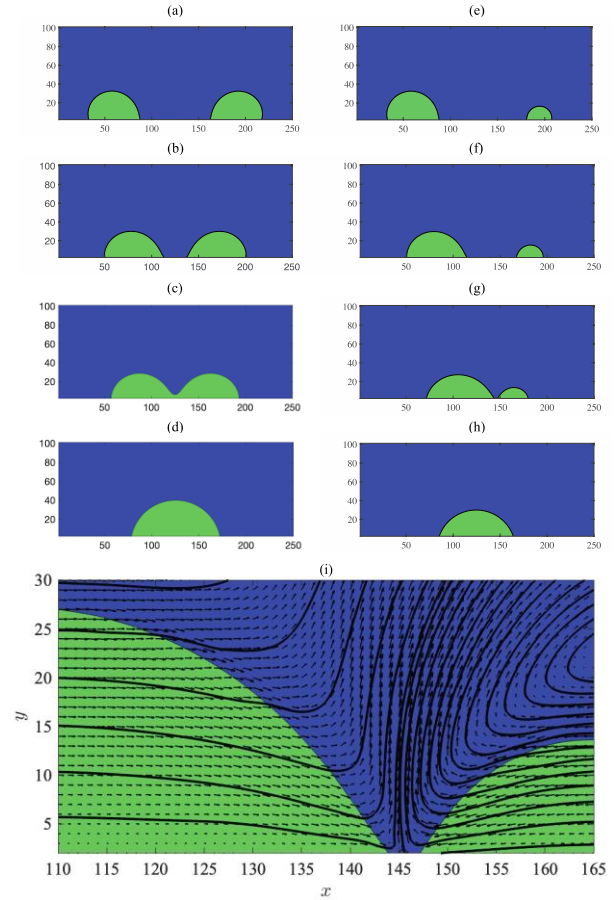


Figure 4. The evolution of the merging droplets on wettability gradient surface, (a)-(d) equal size droplets: $t=5000, 15000, 20000, 50000$; (e-h) different size droplets: $t=5000, 15000, 30000, 50000$; (i) velocity vectors before the different size droplets merge corresponding to (g)

To show this, first equilibrium shapes of columns for several surface energies are given and it is shown that the motion is possible if the surfaces are designed with a surface energy gradient. The same effect is also possible for a wedge shape confinement, but this is a geometric modification for the motion as seen in the self-motion of droplets on conical surfaces and inside wedges (like the self-movement of droplets on cactus spines or liquid columns inside the duck weak).

In Figure 5, the two equilibrium shapes obtained for $\theta_e = 30^\circ$ and $\theta_e = 120^\circ$ are presented in panels (a) and (b), wetting and non-wetting columns, respectively. Because the surface energies are uniform along the walls; the fluid column cannot move without an external force. The wetting gradient is obtained by setting $d\theta_e/dx$ to $(\theta_e^{left} - \theta_e^{right})/n_x$ with $\theta_e^{left} = 120^\circ$, $\theta_e^{right} = 30^\circ$ and $n_x = 250$. This gradient is double the one shown in Figure 3 for 120° - 30° case. As the viscosity ratio and surface tension between liquid and outside fluid are the same, one would then expect

the speed of the column to be twice of the droplet without confinement. The existence of two liquid-solid interfaces doubles the driving force due to hysteresis; however, the viscous losses double as well. Henceforth, the same argument used in section 3.1 applies. But this time, the pressure difference is not along a single interface: the radius of curvature of the leading interface (though uniform along it) is different than the radius of curvature of the trailing interface (again uniform) which can be seen in panels (c)-(e) of Figure 5, this difference generates the Laplace pressure difference from trailing interface to leading interface and this drives the liquid column. The driving mechanisms of a single droplet moving on a wettability gradient and the one confined look similar but they are different in terms of Laplace pressure.

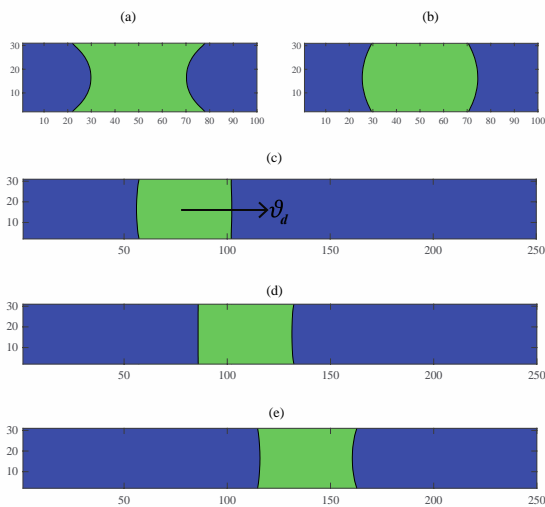


Figure 5. The interface profiles for a droplet confined between walls. (a) Equilibrium shape for $\theta_e = 30^\circ$, (b) Equilibrium shape for $\theta_e = 120^\circ$; the motion of liquid column with surface energy gradient (c) $t=50000$, (d) $t=100000$, (e) $t=150000$

3.4. Influence of channel aspect ratio on the motion of confined droplets

For the motion of interfaces in which there is not much deformation, two-dimensional models could be useful to predict such motions as the aspect ratio of the channel increases. By extending the MRT lattice-Boltzmann solver into three-dimensions with D3Q19 model, the comparison of the three-dimensional liquid columns is shown in Figure 6.

The wetting gradient is set defining $\theta_e^{left} = 120^\circ$, $\theta_e^{right} = 30^\circ$. The aspect ratio is the ratio of the width of the channel (in z -direction) to the height of the channel (in y -direction). To reduce the computational cost, channel length and height are set to $n_x = 150$ and $n_y = 10$, respectively. The width of the channel in the third direction is varied by setting $n_z = 5, 10, 25, 45, 75$. As n_z increases, the aspect ratio increases. The movement of fluid at the central plane approaches the two-dimensional model as the aspect ratio increases.

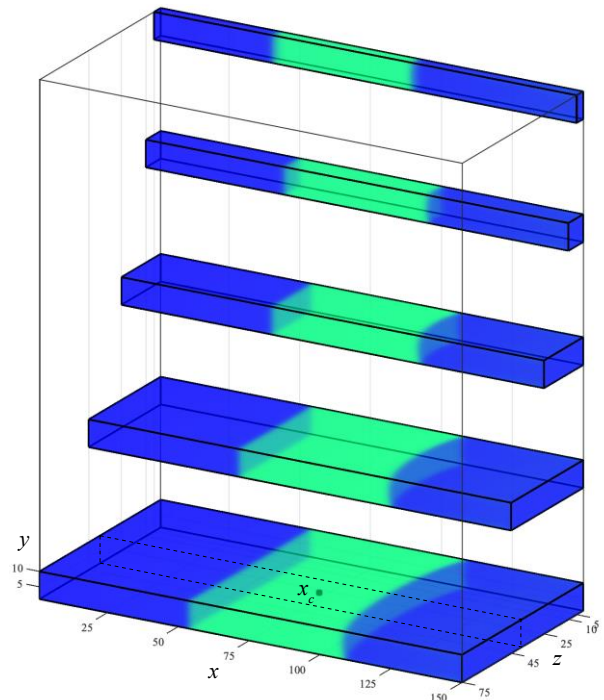


Figure 6. Change of confined droplet profile with aspect ratio at $t=50000$; from top to bottom $n_z=5, 10, 25, 45, 75$. The dashed lines show the central plane with central location x_c

In Figure 7, the time variation of the central locations, x_c (shown in Fig. 6), of the droplet for various aspect ratio channels are shown. For narrow channels (small aspect ratio), the interface motion is much slower than the one predicted with the two-dimensional model; the effects of side walls on the central plane are obvious. The two-dimensional model gives closer predictions compared with the three-dimensional predictions at the central plane (shown in Fig. 7 for $n_z=75$) as the aspect ratio gets larger. This suggests that when the channel aspect ratio is large, the central plane model (two-dimensional) for problems with small deformation could provide useful results with reduced computational cost.

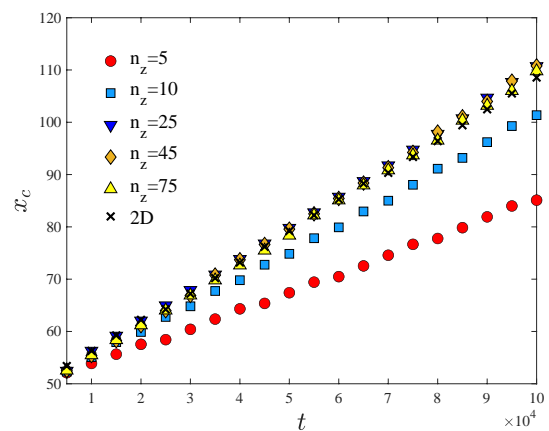


Figure 7. Time variation of x_c for different aspect ratio channels and comparison with two-dimensional prediction

4. Discussion and Conclusion

By modeling the motion of two-phase flows with the MRT binary lattice Boltzmann method, the motion of self-driven droplets with the aid of surface energy gradient is studied. This type of motion is important both in nature and in microfluidic flow manipulation. It is shown how the gradient of such surfaces affects the deformation of the droplets by studying three main problems:

- (i) self-motion of single droplets on surfaces
- (ii) merging of droplets of the same and different size droplets
- (iii) self-driven motion of droplets within confinements

For the three main problems, the MRT lattice-Boltzmann method is found to be useful in modeling the motion of such interfaces over wettability gradient surfaces. With the analyses for these three main problems, it is concluded that the motion of droplets can directionally be controlled by only varying the wettability of the surfaces. The viscosity ratio between the droplet and surrounding medium changes the time scale at which desired motion is completed. By working with different-sized droplets, motivated by the observation of different-sized droplet accumulation on window panes, car glass shields, and surfaces of photo-voltaic panels on rainy days, it is shown that the droplets can be merged at a desired location and gravity may assist in further motion. While it is impossible to provide self-movement of droplets confined within a parallel walled channel without a gradient in the confinement geometry, it is shown that the wetting gradient achieves this movement without altering the confinement geometry. Although the driving mechanisms of a single droplet moving on a wettability gradient and the one confined look similar, they are different in terms of Laplace pressure; the former is due to the pressure variation along the droplet interface, the latter is due to the pressure difference at the two interfaces.

It should finally be noted that the problems analyzed in this study are limited to two-dimensional models (cylindrical droplets). For the confined droplet model, the plane models can be useful for the control of interfaces within large aspect ratio microchannels as shown in the comparison made with the three-dimensional simulation. The results of this study are believed to be the first steps toward understanding such motions and to motivate further studies in three-dimension.

Declaration of Ethical Code

In this study, we undertake that all the rules required to be followed within the scope of the "Higher Education Institutions Scientific Research and Publication Ethics

Directive" are complied with, and that none of the actions stated under the heading "Actions Against Scientific Research and Publication Ethics" are not carried out.

References

- [1] Wu, L., Guo, Z., Liu, W. 2022. Surface behaviors of droplet manipulation in microfluidics devices, *Advances in Colloid and Interface Science*, vol. 308(102770).
- [2] Gosh, A., Ganguly, R., Schutzius, T. M., Megaridis, C. M. 2014. Wettability patterning for high-rate, pumpless fluid transport on open, non-planar microfluidic platforms, *Lab. Chip*, 14, 1538-1550.
- [3] Oliveira, N. M., Vilabril, S., Oliveira, M. B., Reis, R. L., Mano, J. F. 2018. Recent advances on open fluidic systems for biomedical applications: A review, *Mater. Sci. Eng. C. Mater. Biol. Appl.*, 97, 851-863.
- [4] Singh, M., Kondaraju, S., Bahga, S. S. 2018. Mathematical Model for Dropwise Condensation on a Surface with Wettability Gradient, *Journal of Heat Transfer*, 140(071502).
- [5] Hassan, G., Yilbas, B.S., Al-Sharafi, A., Al-Qahtani, H. 2019. Self-cleaning of a hydrophobic surface by a rolling water droplet, *Sci. Rep.*, 9(5744).
- [6] Tenjimbayashi, M., K. Manabe, K. 2022. A review on control of droplet motion based on wettability modulation: principles, design strategies, recent progress, and applications, *Science and Technology of Advanced Materials*, 23(1), 473-497.
- [7] Shen, C., Liu, L., Wu, S., Yao, F., Zhang, C. 2020. Lattice Boltzmann simulation of droplet condensation on a surface with wettability gradient, *Journal of Mechanical Engineering Science*, vol. 234(7),1403-1413.
- [8] Daniel, S., Chaudhury, M. K., Chen, J. C. 2001. Fast Drop Movements Resulting from the Phase Change on a Gradient Surface, *Science*, 291, 633-636.
- [9] Mistura, G., Pierno, M. 2017. Drop mobility on chemically heterogeneous and lubricant-impregnated surfaces, *Adv. in Phys.:* X, 2, 591-60.
- [10] Sadullah, M. S., Kusumaatmaja, H., Launay, G., Parle, J., Ledesma-Aguilar, R., Gizaw, Y., McHale, G., Wells, G. G. 2020. Bidirectional motion of droplets on gradient liquid infused surfaces, *Comm. Phys.*, 3(166).
- [11] Chen, L., Gao, M., Liang, J., Wang, D., Hao, L., Zhang, L. 2022. Lattice Boltzmann simulation of wetting gradient accelerating droplets merging and shedding on a circumferential surface, *Eng. App. of Comp. Fluid Mech.*, 16.

- [12] Qu, J., Yang, X., Wang, Z. 2020. Numerical simulations on the self-motion of droplets in hydrophobic microchannels driven by wettability gradient surfaces, *Int. Comm. in Heat and Mass Trans.*, 119(104961).
- [13] Li, C., Dai, H., Gao, C., Wang, T., Dong, Z., Jiang, L. 2019. Bioinspired inner microstructured tube controlled capillary rise, *PNAS*, vol. 116(26), 12704-12709.
- [14] Moumen, N., Subramanian, R. S., McLaughlin, J. B. 2006. Experiments on the Motion of Drops on a Horizontal Solid Surface Due to a Wettability Gradient, *Langmuir*, 22(6), 2682-2690.
- [15] Raphael, E. 1988. Spreading of droplets on a patchy surface, *C. R. Acad. Sci. Paris*, 306, 751-754.
- [16] Xu, X., Qian, T. 2012. Droplet motion in one-component fluids on solid substrates with wettability gradients, *Phys. Rev. E*, 85(051601).
- [17] Thomas, T. M., Chowdhury, I. U., Dhivyaraja, K., P. Mahapatra, S., Pattamatta, A., Tiwari, M. K. 2021. Droplet Dynamics on a Wettability Patterned Surface during Spray Impact, *Processes*, 9(555).
- [18] Wang, X., Xu, B., Chen, Z. 2020. Numerical simulation of droplet dynamics on chemically heterogeneous surfaces by lattice Boltzmann method, *Int. Jour. of Num. Meth. for Heat & Fluid Flow*, 30(2), 607-624.
- [19] Chowdhury, I. U., Mahapatra, P. S., Sen, A. K. 2019. Self-driven droplet transport: Effect of wettability gradient and confinement, *Physics of Fluids*, 31(042111).
- [20] Chowdhury, I. U., Mahapatra, P. S., Sen, A. K. 2020. Shape evolution of drops on surfaces of different wettability gradients, *Chemical Engineering Science*, 229(116136).
- [21] Gulfam, R., Chen, Y. 2022. Recent Growth of Wettability Gradient Surfaces: A Review, *A Review Research*, 2022(9873075).
- [22] Ding, Y., Yin, L., Dang, C., Liu, X., Xu, J. 2023. Self-climbing of a low surface tension droplet on a vertical conical surface, *Colloids and Surfaces A: Physicochemical and Engineering Aspects*, 658(130670).
- [23] Raj, S. S., Mathew, R. M., Davis, D., Varanakkottu, S. N., Srinivasan, A., & Vinod, T. P. 2023. Facile fabrication of stable wettability gradients on elastomeric surfaces for applications in water collection and controlled cell adhesion. *Soft Matter*, 19(29), 5560-5574.
- [24] Xie, D., Sun, Y., Wu, Y., Wang, K., Wang, G., Zang, F., & Ding, G. 2023. Engineered Switchable-Wettability Surfaces for Multi-Path Directional Transportation of Droplets and Subaqueous Bubbles. *Advanced Materials*, 35(9), 2208645.
- [25] Sung, J., Lee, H. M., Yoon, G. H., Bae, S., & So, H. 2023. One-step fabrication of superhydrophobic surfaces with wettability gradient using three-dimensional printing. *International Journal of Precision Engineering and Manufacturing-Green Technology*, 10(1), 85-96.
- [26] Pooley, C. M., Kusumaatmaja, H., Yeomans, J. M. 2008. Contact line dynamics in binary lattice Boltzmann simulations, *Phys. Rev. E*, 78(056709).
- [27] Briant A. J., Yeomans J. M. 2004. Lattice boltzmann simulations of contact line motion. ii. binary fluids, *Physical Review E*, 69(031603).
- [28] Frisch, U., d'Humières, D., Hasslacher, B., Lallemand, P., Pomeau, Y. and Rivet, J.P. 1987. Lattice gas hydrodynamics in two and three dimensions, *Complex Systems*, 1 (649-707).
- [29] Pooley, C.M., Furtado, K. 2008. Eliminating spurious velocities in the free-energy lattice Boltzmann method, *Physical Review E*, 77(046702).
- [30] Pooley, C. M., Kusumaatmaja, H., Yeomans, J. M. 2009. Modelling capillary filling dynamics using lattice Boltzmann simulations, *Eur. Phys. J. Special Topics*, 171, 63-71.
- [31] Boylu, M. A. 2023. Controlling the Motion of Capillary Driven Interfaces in Channels with Chemical Heterogeneity. İzmir Katip Çelebi University, Graduate School of Natural and Applied Sciences, Master's Thesis, 68 pg., İzmir.
- [32] Broachard, F. 1989. Motions of Droplets on Solid Surfaces Induced by Chemical or Thermal Gradients, *Langmuir*, 5, 432-438.
- [33] Ceyhan, U., Tiktaş, A., Özdoğan, M. 2020. Pinning and depinning of Wenzel-state droplets around inclined steps, *Colloid and Interface Science Communications*, 35(100238)

Appendices

Appendix A. Nomenclature

Greek letters:

γ	surface tension
η	dynamic viscosity
ϕ	order parameter
λ	kinematic viscosity ratio
ρ	fluid density
φ	bulk free energy density
τ	relaxation parameter
θ	contact angle

Roman letters:

a	constant coefficient in Landau model
c	lattice velocity parameter
e	lattice direction
f	distribution function f

F	external body force	Subscripts:	
g	distribution function g	d	droplet
h	height	SV	solid-vapor
M	transformation matrix	SL	solid-liquid
n	number of lattices	c	center
p	pressure	e	equilibrium
P	pressure tensor	o	outside
r	radius of curvature	x	x-direction
\mathbf{r}	lattice position	y	y-direction
S	spreading parameter	Superscripts:	
\mathbf{S}	collision matrix	l	left contact line
t	time	r	right contact line
x	x-direction	$left$	left of the computational domain
y	y-direction	$right$	right of the computational domain